



Research Article

# Mechanism and engineering application of HCL-induced weakening of coal-measure sandy mudstone

Zhao Guofei<sup>a,b,\*</sup>, Ma Dongjuan<sup>a</sup>, Yang Hongyan<sup>b</sup>, Kang Tianhe<sup>c</sup>, Zhang Xiaoyu<sup>b,d</sup>

<sup>a</sup>Department of Safety Engineering, Shanxi Institute of Energy, No. 63, University Street, Higher Education Campus, Shanxi Province, Taiyuan, 030600, China

<sup>b</sup>Department of Technical Center, Shanxi Gowin Construction Technology of Coalbed Gas Co., Ltd, No. 100 Tanghuai Road, Tanghuai Industrial Park, Shanxi Province, Taiyuan, 030032, China

<sup>c</sup>Department of Key Laboratory of In-Situ Modification Mining, Ministry of Education, Taiyuan University of Technology, No. 79, Yingze West Street, Wanbailin District, Shanxi Province, Taiyuan, 030024, China

<sup>d</sup>Department of Emergency Research Institute, Chinese Institute of Coal Science, No. 5 Qingniangou Road, Chaoyang District, Beijing, 100000, China

## ARTICLE INFO

### Keywords:

Acid etching weakening  
Collapse column  
Coal-measure sandy mudstone  
HCl solution

## ABSTRACT

The sandy mudstone within collapse columns is characterized by its density and high mechanical strength, posing significant challenges for direct excavation by coal shearers. Consequently, coal mining operations are impeded by the inability to traverse collapse columns directly. This investigation represents the inaugural elucidation of the chemical weakening mechanism of sandy mudstone subjected to hydrochloric acid (HCl) etching, and it substantiates the practicality of this method within engineering contexts. The employed research methodologies encompass HCl acid etching experiments, rock mechanical property assessments, X-ray diffraction (XRD) analyses, and scanning electron microscopy (SEM) examinations. The findings demonstrate that: The uniaxial compressive strength of sandy mudstone exhibits a negative logarithmic correlation with the volume fraction of the HCl solution; Post-etching, the concentrations of muscovite and kaolinite within the sandy mudstone diminish by 44.74% and 62.96%, respectively, with extensive dissolution of framework particles leading to interconnected pores; The HCl induces a synergistic weakening effect via H<sub>2</sub>O intrusion and H<sup>+</sup> dissolution, substantially degrading cohesion and structural integrity; The engineering applicability indicates that prior to mining, the injection of a 2% HCl solution into the collapse column weakens the rock for over 10 days, enabling the mining face to traverse it directly. A subsequent injection of an optimal amount of Ca(OH)<sub>2</sub> solution into the goaf then neutralizes any residual HCl and mitigates acid corrosion in the mined-out area. This study furnishes a technical strategy for managing complex geological formations, such as waterless collapse columns, in the context of coal mining engineering.

## 1. Introduction

Coal-measure sandy mudstone is the most prevalent lithology encountered in Chinese coal mine collapse columns, and these columns, which penetrate coal seams vertically, present a significant disruption to normal coal mining operations (Yin and Zhang, 2005, and Wu *et al.*, 2020). Compared with other methods, directly passing through collapse columns by cutting rock with coal shearers is the most economical and time-saving approach (Feucht and Logan, 1990, and Lu *et al.*, 2022). However, the challenge lies in the material properties of the rock that forms these collapse columns. Unlike coal bodies, which are relatively soft and exhibit lower structural integrity, coal-measure sandy mudstone has a much higher strength and a strong and cohesive structure (Hu *et al.*, 2025, and Liu *et al.*, 2019). This makes it significantly more difficult to cut through using conventional mining methods (Zhang and Zhang, 2021, and Liu *et al.*, 2011). Therefore, addressing rock weakening is one of the most critical challenges for enabling coal mining faces to effectively pass through waterless collapse columns without risking equipment damage (Zuo *et al.*, 2019). Numerous scholars have investigated the issue of the rock weakening. Previous studies have primarily examined water-induced weakening mechanisms, showing

that water infiltration leads to softening and structural degradation in sandy mudstone (Jiang *et al.*, 2024; Sun *et al.*, 2024; Zhang *et al.*, 2024).

Adding chemical ions to water (especially H<sup>+</sup> ions) intensifies rock deterioration. Acid solutions dissolve carbonate rock minerals to form wormholes, alter surface morphology, and enhance permeability, resulting in significant degradation of mechanical properties (Zhang *et al.*, 2020; Alameedy *et al.*, 2023; Gou *et al.*, 2025). Relevant studies have shown that interaction efficiency between different acid systems and mineral compositions varies remarkably, while the contents of calcite and dolomite are the key factors determining acid treatment efficiency (Abdollahi and Shadzadeh, 2014; Li *et al.*, 2019; Guo *et al.*, 2025; Martyushev *et al.*, 2021). Previous studies focused on carbonate rocks, whereas our work investigates the acid-mechanical coupling behavior of clay-rich coal-measure sandy mudstone. This lithology is primarily composed of clay and clastic minerals, with its strength mainly derived from the cementation effect of the clay mineral components (Fu *et al.*, 2024). Therefore, it is essential to investigate the relationship between the weakening of the rock's mechanical properties under acid corrosion and the corresponding internal microscopic transformations and mineral composition changes.

### \*Corresponding author:

E-mail address: zg-fei@163.com (Z Guofei)

Received: 28 September, 2025 Accepted: 12 January, 2026 Epub Ahead of Print: 04 April, 2026 Published: 16 April, 2026

DOI: 10.25259/JKSUS\_1528\_2025

In this context, laboratory experiments were conducted to examine the changes in compressive strength, stress-strain curves, mineral content, and surface morphology of coal-measure sandy mudstone after immersion in HCl solutions with varying concentrations. The mechanism of HCl-induced acid corrosion in weakening the rock was analyzed. The findings were applied in a field test involving a coal mining working face passing through a collapse column, yielding favorable application results.

2. Materials and Methods

The test sandy mudstone samples were collected from the collapse column in front of the 3405 working face of Tang'an Coal Mine in Gaoping City, Shanxi Province, China. The samples were processed into standard cylindrical specimens with a height of 100 mm and a diameter of 50 mm. In accordance with the Standard Test Methods for Engineering Rock Mass (GB/T50266-2013), these specimens were placed in a vacuum drying oven at temperatures between 105°C and 110°C until they reached a constant weight, after which laboratory tests were conducted. Hydrochloric acid solutions with volume fractions varying from 0% to 6% were synthesized employing concentrated hydrochloric acid and deionized water. All experiments were conducted at a constant temperature of 25°C without stirring to simulate the in-situ underground environment.

A total of 21 experimental schemes were devised, with each scheme consisting of 3 test samples (63 samples in total), as outlined in Table 1. Scheme 1 focused on analyzing the uniaxial compressive strength, stress-strain curve, mineral composition, and surface morphology of the original rock samples. Schemes 2 through 21 primarily examined the uniaxial compressive strength, stress-strain curve, mineral composition, and surface morphology of the rock samples at varying HCl solution volume fractions and immersion times.

The conventional uniaxial compression test for this experiment was conducted using a JL-WAW60 microcomputer-controlled electro-

Table 1. Experimental schemes.

Schemes	Volume fraction/%	pH value/1	Immersion times/d
1	-	-	-
2-5	0	7.00	5, 10, 15, 20
6-9	1	0.92	5, 10, 15, 20
10-13	2	0.62	5, 10, 15, 20
14-17	4	0.32	5, 10, 15, 20
18-21	6	0.14	5, 10, 15, 20

Table 2. Data on the change in compressive strength of rock samples over time after immersion in hcl solutions with different volume fractions.

	0 d	5 d	10 d	15 d	20 d
0% HCl	<u>35.74 ~ 42.15</u> X = 39.00 σ = 3.21	<u>23.78 ~ 32.51</u> X = 28.35 σ = 4.38	<u>15.11 ~ 23.06</u> X = 18.98 σ = 3.98	<u>12.63 ~ 21.96</u> X = 17.03 σ = 4.69	<u>12.97 ~ 18.65</u> X = 15.66 σ = 2.85
1% HCl	<u>35.74 ~ 42.15</u> X = 39.00 σ = 3.21	<u>20.20 ~ 34.11</u> X = 26.97 σ = 6.96	<u>12.35 ~ 20.16</u> X = 16.38 σ = 3.91	<u>10.13 ~ 15.48</u> X = 13.12 σ = 2.73	<u>10.51 ~ 14.23</u> X = 12.84 σ = 2.03
2% HCl	<u>35.74 ~ 42.15</u> X = 39.00 σ = 3.21	<u>23.34 ~ 26.59</u> X = 25.02 σ = 1.63	<u>11.80 ~ 17.99</u> X = 14.61 σ = 3.13	<u>9.43 ~ 14.24</u> X = 11.85 σ = 2.41	<u>9.29 ~ 13.76</u> X = 11.63 σ = 2.24
4% HCl	<u>35.74 ~ 42.15</u> X = 39.00 σ = 3.21	<u>19.58 ~ 24.69</u> X = 22.85 σ = 2.84	<u>10.66 ~ 15.83</u> X = 13.25 σ = 2.59	<u>10.19 ~ 11.54</u> X = 10.98 σ = 0.70	<u>10.04 ~ 11.27</u> X = 10.81 σ = 0.67
6% HCl	<u>35.74 ~ 42.15</u> X = 39.00 σ = 3.21	<u>18.36 ~ 23.75</u> X = 21.66 σ = 2.89	<u>8.34 ~ 5.37</u> X = 12.22 σ = 3.57	<u>9.15 ~ 11.45</u> X = 10.46 σ = 1.18	<u>8.33 ~ 10.95</u> X = 9.92 σ = 1.39

Note: X̄ represents the average value, σ represents the standard deviation.

hydraulic servo universal testing machine, with a loading rate of 0.005 mm/s. The mineral composition of the rock samples was determined using a D/MAX-2700 X-ray diffraction spectrometer, operating at a scanning speed of 8 °/min and a 2θ scanning range of 5° - 85°. The surface morphology of the rock samples was examined with a LEO435VP scanning electron microscope, which features an electron gun filament diameter of 50 μm, an operating voltage range of 1 to 30 kV, and a magnification capability of 100,000 to 400,000 times.

3. Results and Discussion

3.1 Compressive strength

The test results of the compressive strength of coal-measure sandy mudstone samples after immersion in HCl solutions with different volume fractions for different durations are presented in Table 2 and Fig. 1. The following observations can be drawn from the data: The compressive strength of the specimens decreases significantly after immersion in HCl solution. Specifically, after immersion in HCl solution with a volume fraction of 6%, the compressive strength of the specimens is 39.00 MPa (0 d), 21.66 MPa (5 d), 12.22 MPa (10 d), 10.46 MPa (15 d), and 9.92 MPa (20 d) respectively; the decrease ranges are 0%, 44.45%, 68.67%, 73.18%, and 74.56% respectively; the reduction rates at each stage are 44.45% (0-5 d), 43.58% (5-10 d), 14.40% (10-15 d), and 5.16% (15-20 d) respectively. During the 0-10 day immersion period, the compressive strength of the specimens decreases sharply; during the 10-20 day, the reduction rate stabilizes.

Taking the 15 days immersion as an example (Fig. 2), the compressive strength of rock samples decreases with increasing HCl solution volume fraction. This change follows a negative logarithmic trend:  $\sigma_c = -1.67 \cdot \ln(\varphi + 0.15) + 13.63$  (R<sup>2</sup>= 0.984). This behavior can be attributed to the initial high concentration of H<sup>+</sup> ions and mineral content, which allows the HCl solution to fully interact with the mineral components of the rock sample, resulting in a more vigorous reaction. As the H<sup>+</sup> ions or mineral components are consumed, the intensity of the reaction decreases, leading to a slower rate of decline in compressive strength.

3.2 Stress-strain curve

The stress-strain curves of the rock samples after being immersed in HCl solutions with different volume fractions for 20 days are shown in Fig. 3.

1) Pore and fracture compaction stage: As stress increases, the  $\frac{d\sigma}{d\varepsilon}$  value increases accordingly, and the curve in this stage exhibits a concave shape ( $\frac{d^2\sigma}{d\varepsilon^2} > 0$ ).

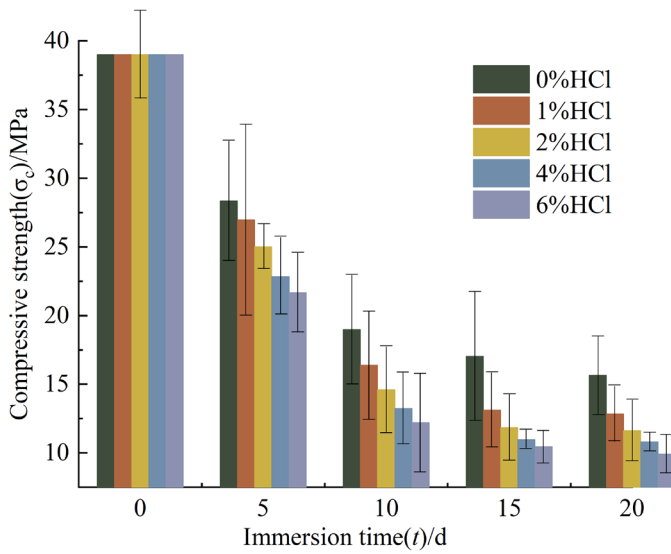


Fig. 1. Bar chart of the compressive strength of specimens changing with time after immersion in HCl solution.

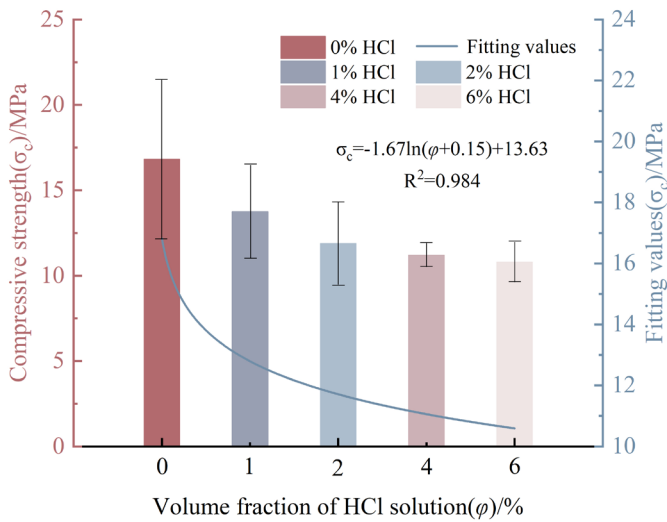


Fig. 2. Changes of compressive strength of rock samples with volume fraction after immersion for 15 days.

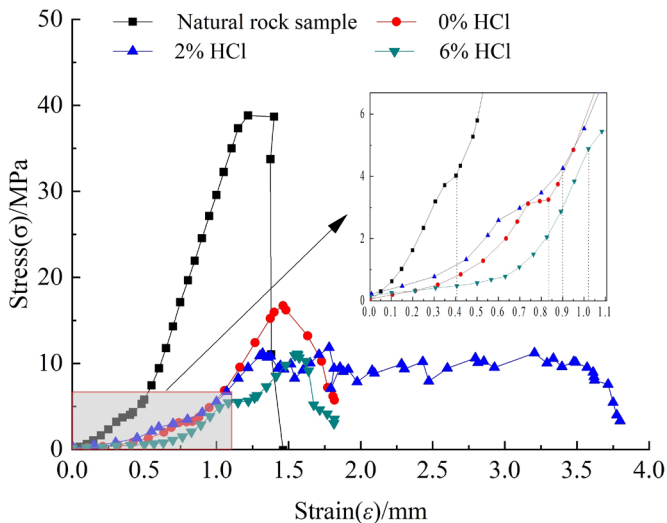


Fig. 3. Uniaxial compression stress-strain curves of rock samples after 20-day immersion in HCl solutions with different volume fractions.

The compaction stage of natural rock samples is very brief, with deformation quickly entering the elastic deformation stage. In contrast, rock samples immersed in HCl solution experience a prolonged compaction stage before entering the elastic deformation phase. When stress is applied, the initially open structural surfaces or microcracks in the rock sample gradually close. Acid corrosion weakens the rock sample by increasing pore size, enhancing pore connectivity, and improving compressibility. As a result, the specimen exhibits significantly greater deformation in this stage compared to the natural state.

The initial elastic modulus of the stress-strain curve reflects the development and connectivity of the specimen's pores. The observed significant reduction in the initial elastic modulus of the specimen after immersion in HCl solution indicates that the acid etching effect of the solution increases the porosity of the rock sample.

2) Elastic Deformation Stage: This stage is characterized primarily by elastic compression deformation, where the stress-strain curve exhibits a linear relationship.

As illustrated in Fig. 3, the initial elastic modulus of the specimen is 5083 MPa. After immersion in 0%, 2%, and 6% HCl solutions for 20 days, the elastic modulus of the specimens is 2446 MPa, 1796 MPa, and 1798 MPa, respectively. The elastic modulus under 2% HCl solution decreases by 64.67%. This substantial reduction indicates a significant acid-weakening effect of the HCl solution on the specimen, which is attributed to the cement composition of sandy mudstone (Hutchinson et al., 1993). However, the elastic modulus values for specimens treated with 2% and 6% HCl solutions are relatively similar. Thus, within the studied volume fraction range, once the HCl concentration exceeds 2%, there is no substantial difference in its effect on the elastic modulus. Therefore, the magnitude of the elastic modulus serves as an indicator of the degree of acid corrosion weakening inflicted by HCl solutions of varying concentrations. A lower elastic modulus corresponds to a greater extent of weakening.

3) Unstable fracture development stage: the  $\frac{d\sigma}{d\varepsilon}$  value decreases with increasing stress, and the curve in this stage exhibits a convex shape  $\left(\frac{d^2\sigma}{d\varepsilon^2} < 0\right)$ .

The failure strain of each specimen immersed in HCl solutions of varying concentrations exceeds that of the natural state, indicating a pronounced influence of the acid-weakening effect on the initiation and development of microcracks within the specimens. Analysis of the stress-strain curves reveals that the microstructural alterations induced by acid corrosion significantly affect the behavior of the specimens at this stage. This stage is mainly caused by the occurrence, development and penetration of microcracks. The yield point is most pronounced in the stress-strain curve of coal-measure sandy mudstone treated with 6% HCl solution, which directly suggests that the acid-weakening effect on the rock's microstructure is most significant at this concentration.

4) Post-fracture stage: the curve is approximately vertical, and the stress decreases rapidly.

Compared to natural specimens, those immersed in HCl solution exhibit greater stability after the peak, indicating that the immersed specimens become less brittle and more ductile. However, the acid corrosion weakening effect does not alter the fundamental nature of the sandy mudstone's brittle failure. Preliminary analysis suggests that after HCl dissolves the carbonate cement in sandy mudstone, a small number of tiny pores are formed. These pores can release the internal primary stress of the rock, reduce brittle failure caused by stress concentration, and make it easier for the rock to maintain structural integrity during the residual stage. Meanwhile, after the dissolution of carbonate cement, the contact mode between siliceous sand grains changed from "cemented connection" to "mechanical interlocking" (Bruthans et al., 2014). The frictional force generated by mechanical interlocking is higher than the original cementation force, which further enhances the residual strength (Xiao et al., 2017).

### 3.3 Inorganic mineral composition

The inorganic mineral composition of rock samples immersed in HCl solutions with varying concentrations for 20 days was determined

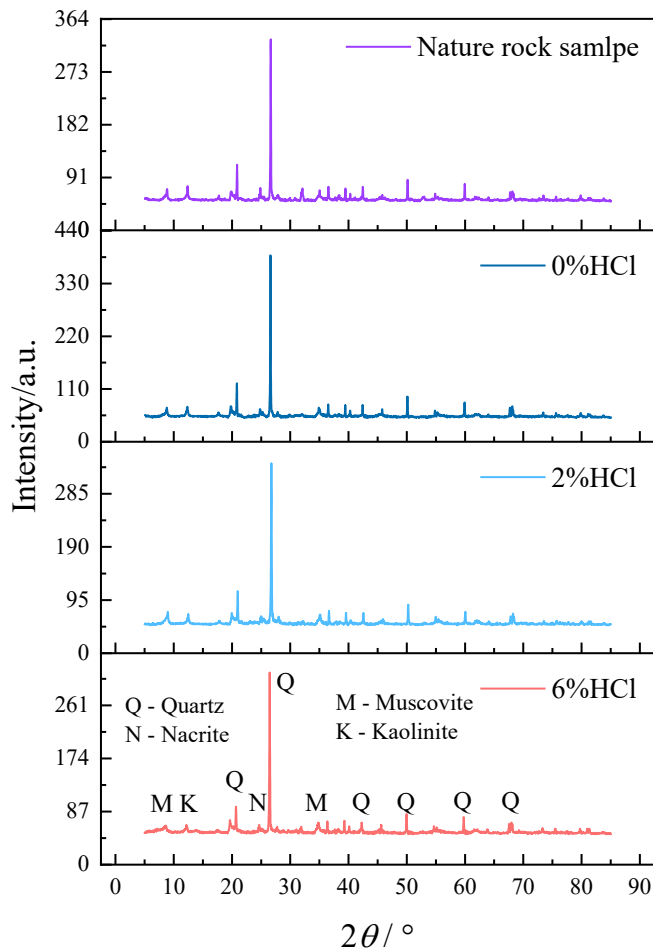


Fig. 4. XRD of untreated samples and rock samples immersed in HCl solutions with different volume fractions for 20 days.

using X-ray diffraction (XRD). 3 samples were measured under different conditions. Fig. 4 presents the XRD patterns of the samples both before and after immersion in the HCl solution. The adiabatic method was employed for quantitative analysis of the mineral composition, and the primary inorganic mineral composition of rock samples before and after immersion in the HCl solution was recorded (Table 3 and Fig. 5).

It can be observed that after the samples were immersed in HCl solutions with different volume fractions, the contents of primary

**Table 3.**  
Primary inorganic mineral composition of rock samples before and after immersion in HCl solution.

	Quartz/%	Muscovite/%	Kaolinite/%	Nacrite/%
Natural rock samples	76.3 ~ 81.0 $\bar{X} = 78.2$ $\sigma = 2.44$	8.5 ~ 13.7 $\bar{X} = 11.4$ $\sigma = 2.65$	3.9 ~ 7.3 $\bar{X} = 5.4$ $\sigma = 1.73$	3.8 ~ 7.1 $\bar{X} = 5.0$ $\sigma = 2.12$
0%HCl	78.3 ~ 85.3 $\bar{X} = 81.6$ $\sigma = 3.52$	8.7 ~ 12.3 $\bar{X} = 10.3$ $\sigma = 1.83$	1.7 ~ 5.4 $\bar{X} = 3.4$ $\sigma = 1.87$	3.8 ~ 5.9 $\bar{X} = 4.7$ $\sigma = 1.08$
2%HCl	83.7 ~ 88.4 $\bar{X} = 85.8$ $\sigma = 2.39$	6.2 ~ 8.9 $\bar{X} = 7.4$ $\sigma = 1.37$	1.3 ~ 3.8 $\bar{X} = 2.5$ $\sigma = 1.25$	2.4 ~ 6.6 $\bar{X} = 4.3$ $\sigma = 2.13$
6%HCl	84.1 ~ 88.8 $\bar{X} = 86.3$ $\sigma = 2.32$	4.6 ~ 8.5 $\bar{X} = 6.3$ $\sigma = 1.93$	1.7 ~ 2.4 $\bar{X} = 2.0$ $\sigma = 0.36$	3.7 ~ 7.6 $\bar{X} = 5.4$ $\sigma = 1.87$

Note:  $\bar{X}$  represents the average value,  $\sigma$  represents the standard deviation.

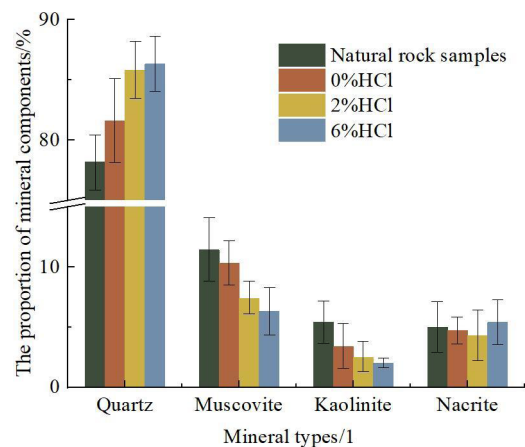
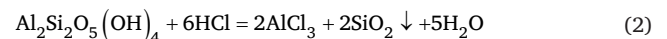
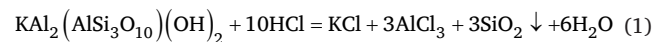


Fig. 5. Bar chart of changes in main inorganic mineral components of samples before and after immersion in HCl solution.

inorganic minerals changed to varying degrees. The quartz content increased by 10.36%, muscovite and kaolinite decreased by 44.74% and 62.96% respectively, while the nacrite content remained basically unchanged. The chemical equations for the reactions of muscovite  $(KAl_2(AlSi_3O_{10})(OH)_2)$  and kaolinite  $(Al_2Si_2O_5(OH)_4)$  with HCl are shown in Eq. (1) and (2) (Awad et al., 2017). 1 mol of muscovite can consume 10 mol of HCl, producing 1 mol of KCl, 3 mol of  $AlCl_3$  and 3 mol of  $SiO_2$ . 1 mol of kaolinite consumes 6 mol of HCl, producing 2 mol of  $AlCl_3$  and 2 mol of  $SiO_2$ . Soluble salts such as KCl and  $AlCl_3$  produced by the reaction migrate with the solution, while  $SiO_2$  remains as an inert precipitate. This dissolution damages the connections between rock particles or crystals, causing damage to the rock's microstructure, further reduces the continuity and integrity of the samples, and ultimately renders the rock blocks loose and brittle. Macroscopically, this is characterized by a decrease in mechanical strength.



### 3.4 Microstructural characteristics

Natural rock samples, as well as rock samples soaked in HCl solutions with volume fractions of 0% and 2% for 20 days, were observed for their surface morphologies using a scanning electron microscope (SEM), as shown in Fig. 6.

Fig. 6(a) shows that in the coal-measure sandy mudstone sample, there are large aggregates composed of quartz particles, which are intertwined with muscovite and kaolinite in a flaky and flocculent structure, forming a relatively dense rock mass structure. Fig. 6(b) shows that after the rock sample was soaked in the 0% HCl solution, its original microstructure was significantly damaged. Larger framework particles were dissolved and stripped, resulting in the formation of dissolved pores, pore expansion, and structural loosening. The diameter of dissolved pores ranges from 10 to 27  $\mu m$ , with an average value of 18  $\mu m$ . Fig. 6(c) indicates that after being soaked in the 2% HCl solution, the connections between the coarse particles, muscovite, and kaolinite in the rock sample were further weakened. The phenomena of pore dissolution and connectivity were obvious, and the flaky structure of muscovite was clearly visible. This flaky structure is prone to sliding between faces under external forces, leading to further deterioration of the rock mass structure. The diameter of connected pores ranges from 34 to 88  $\mu m$ , with an average value of 63.75  $\mu m$ . Analysis of these results shows that  $H^+$  ions in the HCl solution can effectively dissolve muscovite and kaolinite in the coal-measure sandy mudstone. Larger framework particles are dissolved and stripped, which damages the connections between rock particles, forms dissolved pores and connected pores, causes damage to the rock's microstructure, weakens

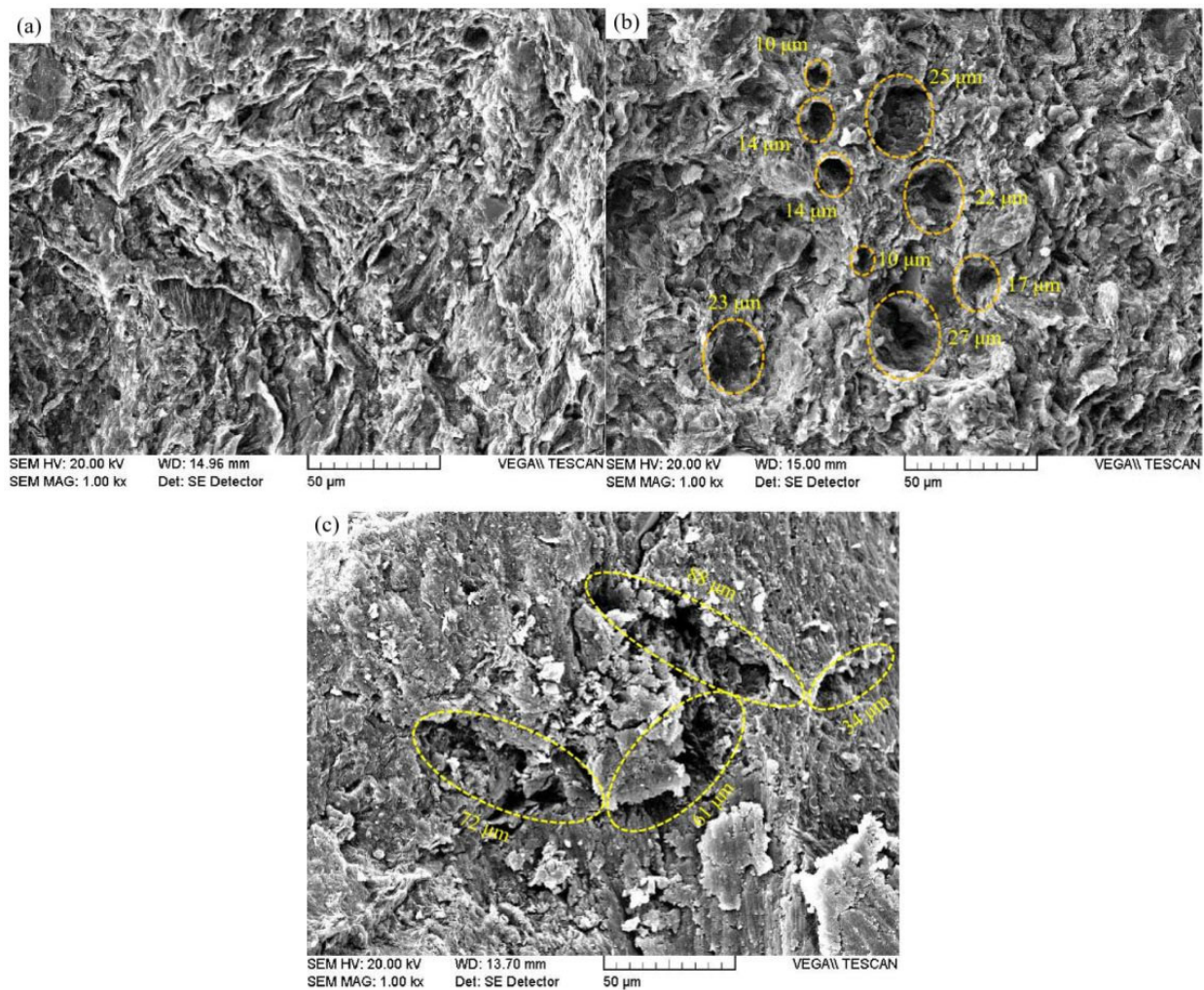


Fig. 6. SEM images of rock samples before and after HCl solution immersion. [(a) Natural rock sample(X1000); (b) Rock sample after 0% HCl solution immersion (X1000); (c) Rock sample after 2% HCl solution immersion(X1000)]; (b,c) Yellow circle highlight the range of dissolved pores.

the internal cohesion of the rock samples, and ultimately reduces their mechanical strength

### 3.5 HCl-induced weakening mechanism

Coal-measure sandy mudstone constitutes a sedimentary rock that emerges from the consolidation of rigid framework particles, such as quartz and feldspar, and clay minerals, including muscovite and kaolinite. The mechanical strength of this rock is contingent upon the interparticle cementation and the structural integrity (Fu et al., 2022). The weakening effect of the rock by hydrochloric acid (HCl) solution is a complex process that involves the synergistic actions of water molecule penetration and the activity of hydrogen ions ( $H^+$ ). Capillary action facilitates the infiltration of water molecules into the rock's pores, where they interact with the surfaces of clay minerals. Notably, minerals such as kaolinite possess numerous hydroxyl groups ( $-OH$ ) on their surfaces; water molecules establish new hydrogen bonds with these groups, supplanting the preexisting hydrogen bonds between mineral particles and thus diminishing the cohesion of hydrogen bonds among them (Tunega et al., 2004). Concurrently, the polarity of these molecules fosters electrostatic interactions with charged ions on the mineral surfaces, such as  $Al^{3+}$  in kaolinite and  $K^+$  in muscovite, thereby attenuating the inherent van der Waals forces between particles. Upon entering the rock, these molecules infiltrate the interlayer spaces of clay minerals, causing them to swell (Pang et al., 2020). This swelling exerts tension on the cementation interfaces between particles, leading to the expansion of micro-pores within the initially dense microstructure. Hydrogen ions ( $H^+$ ) penetrate the interior of the pores and selectively

dissolve cemented clay minerals (muscovite, kaolinite) and certain auxiliary framework minerals (Belver et al., 2002, and Van 1963). The soluble  $Al^{3+}$  ions,  $K^+$  ions, and  $SiO_2$  colloids generated by the reaction between hydrogen ions and minerals are transported by the solution traversing the rock's pores and are subsequently leached out, resulting in the formation of larger dissolution cavities (Xiao et al., 2025). Ultimately, the rock's microstructure evolves from a dense "framework-cement matrix" system to a more porous system characterized by "isolated framework particles alongside numerous dissolution cavities," which significantly diminishes its mechanical strength.

## 4. Field Application and Engineering Verification

### 4.1 Geological background

The 3405 coal mining face of Tang'an Coal Mine in Gaoping City, Shanxi Province, is located within the middle deformation zone between the north-south compressional deformation zone of the North China Plate and the Lüliang-Taihang Fault Block (Fig. 7). This compressional force transformed the originally nearly E-W trending structures of the Indosinian period into a more prominent northeastward strike (Fig. 8a). During the Miocene epoch, the continuous convergence of the Indian Plate and the Eurasian Plate drove the gradual uplift of the Taihang Mountains, and concurrently, the stress direction shifted from the original NW-SE to NNW-SSE (Fig. 8b). Under the action of tectonic forces, the dissolution of the underlying rock layers formed the collapse column in this coal mining area.

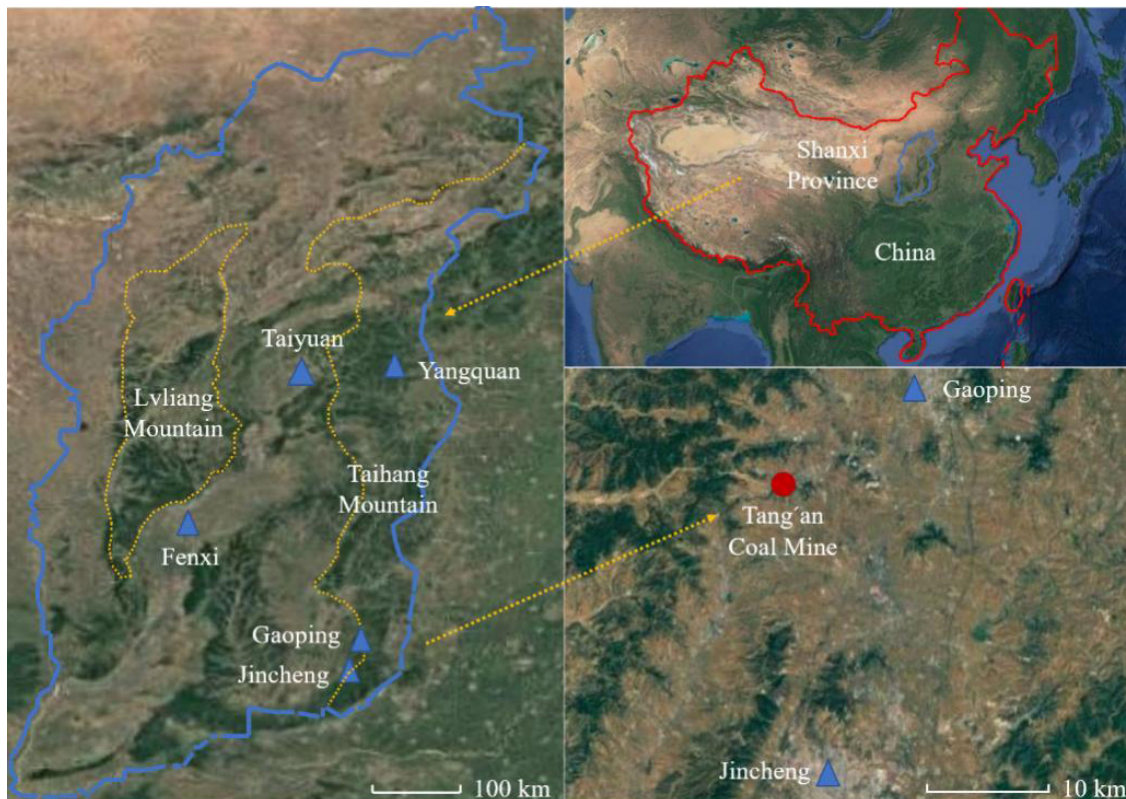


Fig. 7. Location of Tang'an coal mine, Shanxi Province, China.

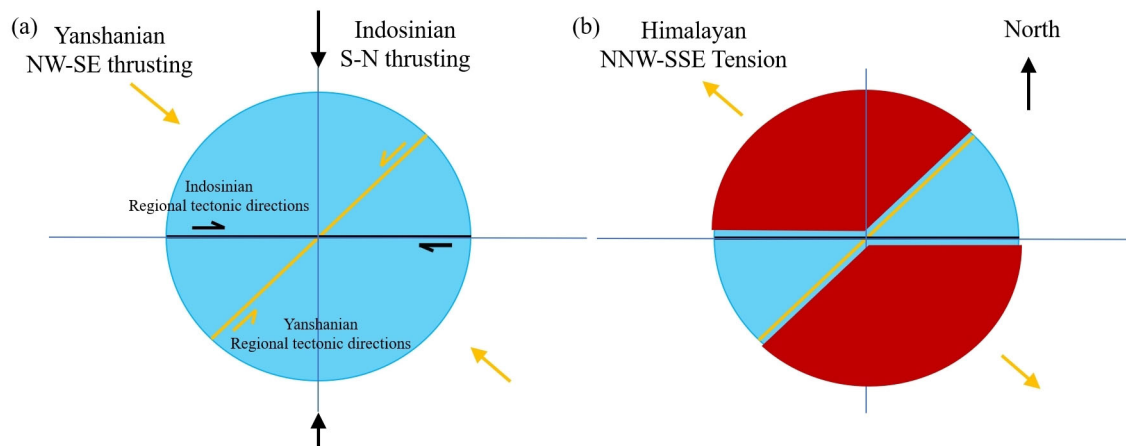


Fig. 8. Stress field in North China.

4.2 Overview of collapse column

The collapse column is located ahead of the 3405 coal mining face in Tang'an Coal Mine, Gaoping City, Shanxi Province. It is roughly elliptical, with a major axis of approximately 25 meters and a minor axis of about 17 meters (Fig. 9). When the coal mining face approaches or exposes the collapse column, considerable challenges may arise both in terms of operational safety and equipment operating efficiency.

4.3 Implementation parameters and effects

Grouting holes were drilled into the collapse column rock from the 3405 return airway, with the following borehole parameters: a diameter of 42 mm, a spacing of 6 m between adjacent holes, and the grouting holes positioned 2 m from the bottom and 1 m from the top of the airway. Based on laboratory test results, a HCl solution with a 2% volume fraction was selected for injection. Depending on the specific treatment requirements of different areas within the collapse column, the injection volume of the acid solution for each grouting

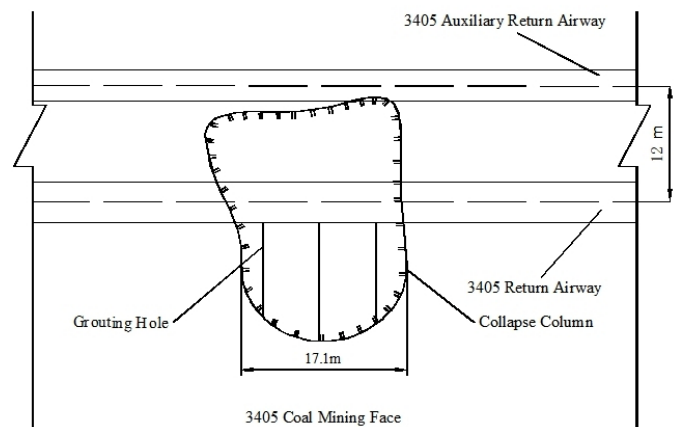


Fig. 9. Diagram of collapse column location and grouting hole layout ahead of the 3405 coal mining face.

**Table 4.** Comparison of mining face process parameters before and after rock softening with HCl solution.

	Uniaxial compressive strength of rock/MPa	Cutting depth of shearer/m	Advancing speed/m/d	Breakthrough time/d
Before softening	35.74 ~ 42.15 $\bar{X} = 39.00$ $\sigma = 3.21$	Cannot be directly cut	-	≈30
After softening	10.26 ~ 14.51 $\bar{X} = 12.25$ $\sigma = 2.14$	0.8	3.2	5.3

Note:  $\bar{X}$  represents the average value,  $\sigma$  represents the standard deviation.

hole was controlled between 2 and 4 m<sup>3</sup>. Considering that the 3405 coal mining face advances at a rate of 3.2 m/d, grouting was required to be completed when the mining face was still 48 meters away from the collapse column—this was to ensure that the HCl solution had no less than 10 days to etch the collapse column rock.

Upon conducting on-site sampling and subsequent laboratory analyses, the uniaxial compressive strength of three samples subjected to softening by hydrochloric acid (HCl) solution was determined. The data comparing the mining face process parameters before and after the rock softening are presented in Table 4. Upon the 3405 coal mining face advancing to the collapse column, the average uniaxial compressive strength of the HCl-etched sandy mudstone was observed to be 12.25 MPa. This figure represents a 68.59% decrease from the uniaxial compressive strength of the pristine rock and is comparable to that of coal. Following the softening process, the shearer was able to directly cut through the rocks within the collapse column. The duration required for the coal mining face to traverse the collapse column experienced a reduction of 82.33%. However, taking into account the looseness of the collapse column rock, advance support measures should be implemented to prevent roof falls in the coal mining face. Upon the coal mining face traversing the collapse column, a Ca(OH)<sub>2</sub> solution with a 10% volume fraction was systematically infused into the goaf at a rate of 0.64 m<sup>3</sup>/d to maintain the residual solution's pH value at approximately 7, thereby mitigating the acid corrosive impact of the HCl solution on the mining area.

During the operation, no accidents occurred at the 3405 coal mining face, ultimately achieving dual benefits of technological innovation and economic efficiency. By conducting acid etching and weakening treatment on the sandy mudstone of the collapse column, the coal mining face could continue advancing at the standard speed, which not only minimized downtime to the greatest extent but also ensured the cost-effectiveness of the coal mining process. This case fully verifies the practical application value of the rock acid etching and weakening technology in improving the efficiency and safety of coal mining operations. In particular, it provides a feasible technical approach for addressing complex geological structures such as collapse columns.

## 5. Conclusions

The mechanism of HCl-induced weakening of coal-measure sandy mudstone is the synergistic effect of H<sub>2</sub>O molecule intrusion and H<sup>+</sup> ion dissolution. H<sub>2</sub>O molecules weaken the cohesion within the rock mass structure, while H<sup>+</sup> ions damage the cementitious bridges and skeletal support, ultimately resulting in a significant reduction in its mechanical strength. The uniaxial compressive strength of the rock exhibits a negative logarithmic relationship with the concentration of the hydrochloric acid solution  $\sigma_c = -1.67 \cdot \ln(\varphi + 0.15) + 13.63$ .

In engineering practice, the rock acid etching weakening technology was applied to the 3405 coal mining face of Tang'an Coal Mine. 2% HCl solution was injected into the collapse column rock, with a weakening period of no less than 10 days, enabling the mining face to pass through the collapse column directly. Additionally, an appropriate amount of Ca(OH)<sub>2</sub> solution was injected into the goaf to neutralize residual HCl and mitigate acid corrosion in the mining area. This application verifies the technology's practical value in typical coal mine projects.

This technology is suitable for rock weakening treatment in complex geological structures such as waterless collapse columns, but should be used with caution in coal mining areas adjacent to aquifers. Future applications should incorporate real-time monitoring of the HCl-induced weakening effect to dynamically adjust implementation parameters, while enhancing residual HCl testing in goafs to ensure no environmental harm.

## CRedit authorship contribution statement

**Zhao Guofei:** Conceptualization, methodology; **Ma Dongjuan:** Visualization, investigation, writing – original draft preparation; **Yang Hongyan:** Validation, formal analysis, writing – review & editing; **Kang Tianhe:** Conceptualization, supervision; **Zhang Xiaoyu:** Software, writing – review & editing.

## Declaration of competing interest

The authors declare that they have no competing financial interests or personal relationships that could have influenced the work presented in this paper.

## Data availability

All data used in this manuscript have been presented within the article.

## Declaration of generative AI and AI-assisted technologies in the writing process

The authors confirm that there was no use of artificial intelligence (AI)-assisted technology for assisting in the writing or editing of the manuscript and no images were manipulated using AI.

## Acknowledgment

We would like to express our gratitude to Associate Professor Pang Jiewen of Taiyuan University of Science and Technology and Associate Professor Chen Chen of Shanxi Institute of Energy for their invaluable contributions to the writing of this manuscript.

## Funding

Shanxi Provincial Special Guidance Project for the Transformation of Scientific and Technological Achievements (No. 202304021301017), Central Government-Guided Local Science and Technology Development Fund of Shanxi Province (No. YDZJSX2024C036), and Fundamental Research Program of Shanxi Province (No. 202403021221354).

## References

- Abdollahi, R., Shadizadeh, S.R., 2014. The effect of spent acid on carbonate rock wettability during a matrix acidizing treatment. *Pet Sci Technol* 32, 450-454. <https://doi.org/10.1080/10916466.2011.590841>
- Alameedy, U., Fatah, A., Abbas, A.K., Al-Yaseri, A., 2023. Matrix acidizing in carbonate rocks and the impact on geomechanical properties: A review. *Fuel* 349, 128586. <https://doi.org/10.1016/j.fuel.2023.128586>
- Awad, M.E., López-Galindo, A., Setti, M., El-Rahmany, M.M., Iborra, C.V., 2017. Kaolinite in pharmaceuticals and biomedicine. *Int J Pharm* 533, 34-48. <https://doi.org/10.1016/j.ijpharm.2017.09.056>
- Belver, C., Bañares Muñoz, M.A., Vicente, M.A., 2002. Chemical activation of a kaolinite under acid and alkaline conditions. *Chem Mater* 14, 2033-2043. <https://doi.org/10.1021/cm0111736>
- Bruthans, J., Soukup, J., Vaculikova, J., Filippi, M., Schweigstilova, J., Mayo, A.L., Masin, D., Kletetschka, G., Rihosek, J., 2014. Sandstone landforms shaped by negative feedback between stress and erosion. *Nature Geosci* 7, 597-601. <https://doi.org/10.1038/ngeo2209>
- Feucht, L.J., Logan, J.M., 1990. Effects of chemically active solutions on shearing behavior of a sandstone. *Tectonophysics* 175, 159-176. [https://doi.org/10.1016/0040-1951\(90\)90136-v](https://doi.org/10.1016/0040-1951(90)90136-v)
- Fu, H.Y., Long, B., Shi, Z.N., Zeng, L., Gao, Q.F., 2022. Study on the mechanical properties and meso-mechanism of silty mudstone under acid corrosion. *Chin J Underground Space Eng* 18, 1441-1451. <https://doi.org/10.13721/j.cnki.dsy.2022.05.014>

- Fu, H., Yu, X., Zeng, L., Luo, J., Liu, J., 2024. Mechanical properties and damage constitutive model of silty mudstone under heating and water-cooling cycles. *Acta Geotech* 19, 5031-5050. <https://doi.org/10.1007/s11440-023-02225-4>
- Gou, B., Liu, Z., Zhou, J., Xu, K., Xiao, B., Pu, K., Guo, J., 2025. Experimental and modeling study on the acid-etching and conductivity of hydraulic fractures in carbonate rocks: A critical review. *Geoenergy Sci Eng* 245, 213517. <https://doi.org/10.1016/j.geoen.2024.213517>
- Guo, G., Zhang, Z., Liu, P., Guo, Y., Ye, Y., Liu, Y., 2025. Experimental study on solid acid systems for acid fracturing in ultrahigh-temperature carbonate reservoirs. *ACS Omega* 10, 45309-45322. <https://doi.org/10.1021/acsomega.5c04835>
- Hu, M., Xu, W.Y., Wang, H., Huang, W., Ning, Y., Zhang, T., 2025. Experimental analysis and modeling study of the coupled elastoplastic damage model for sandy mudstone. *Bull Eng Geol Environ* 84, 243. <https://doi.org/10.1007/s10064-025-04258-3>
- Hutchinson, A.J., Johnson, J.B., Thompson, G.E., Wood, G.C., Sage, P.W., Cooke, M.J., 1993. Stone degradation due to wet deposition of pollutants. *Corros Sci* 34, 1881-1898. [https://doi.org/10.1016/0010-938x\(93\)90025-c](https://doi.org/10.1016/0010-938x(93)90025-c)
- Jiang, N., Yin, D., Jiang, X., Gao, Z., Yang, S., Jia, C., 2024. Experimental study on the deterioration of mechanical properties of sandy mudstone under different water-gas interactions. *Heliyon* 10, e30667. <https://doi.org/10.1016/j.heliyon.2024.e30667>
- Li, Q., Chen, W., Lu, Y., Xiao, Q., 2019. Etched surface morphology analysis experiments under different reaction rates. *J Petroleum Sci Eng* 172, 517-526. <https://doi.org/10.1016/j.petrol.2018.09.063>
- Liu, H., Zhang, D., Zhao, H., Chi, M., Yu, W., 2019. Behavior of weakly cemented rock with different moisture contents under various tri-axial loading states. *Energies* 12, 1563. <https://doi.org/10.3390/en12081563>
- Liu, S., Du, C., Cui, X., Gao, K., 2011. Characteristics of different rocks cut by helical cutting mechanism. *J Cent South Univ Technol* 18, 1518-1524. <https://doi.org/10.1007/s11771-011-0868-2>
- Lu, C.J., Xu, J.P., Wang, T.M., 2022. Safety mining guarantee technology for coal face crossing collapse column based on grouting reinforcement - a comparative study using UDEC and FLAC3D numerical simulation. *Fresenius Environ Bull* 31 5176-5184. <https://doi.org/10.18596/feb.31.5.5176>
- Martyushev, D.A., Govindarajan, S.K., Li, Y., Yang, Y., 2022. Experimental study of the influence of the content of calcite and dolomite in the rock on the efficiency of acid treatment. *J Petroleum Sci Eng* 208, 109770. <https://doi.org/10.1016/j.petrol.2021.109770>
- Pang, J., Liang, Y., Masuda, Y., Matsuoka, T., Zhang, Y., Xue, Z., 2020. Swelling phenomena of the nonswelling clay induced by CO<sub>2</sub> and water cooperative adsorption in Janus-surface micropores. *Environ Sci Technol* 54, 5767-5773. <https://doi.org/10.1021/acs.est.0c00499>
- Sun, X., Shi, F., Zhu, M., Ding, J., He, L., Li, Z., Zhang, T., Miao, C., 2024. Microscopic mechanisms and acoustic emission characteristics of sandy mudstone under different water saturations. *KSCE J Civil Eng* 28, 471-483. <https://doi.org/10.1007/s12205-023-1089-6>
- Tunega, D., Gerzabek, M.H., Lischka, H., 2004. Ab initio molecular dynamics study of a monomolecular water layer on octahedral and tetrahedral kaolinite surfaces. *J Phys Chem B* 108, 5930-5936. <https://doi.org/10.1021/jp037121g>
- Van Olphen, H., 1963. Swelling of clay minerals and associated phenomena in porous media. *Clays Clay Miner* 11, 204-219. <https://doi.org/10.1346/CCMN.1963.0110308>
- Wu, B., Kong, J., Dong, S., 2020. Seismic attribute method for concealed collapse column identification in coal fields. *Acta Geod Geophys* 55, 11-21. <https://doi.org/10.1007/s40328-019-00278-0>
- Xiao, C., Deng, S., Huang, Z., Zuo, H., 2017. Numerical and experimental investigation of the argillaceous sandstone mechanical properties by the discrete element method. In: *AER-Advances in Eng Res* 124, 127-134. <https://doi.org/10.2991/isaeece-17.2017.24>
- Xiao, S., Qu, J., Tang, Y., Ding, W., Liu, X., 2025. Electric-field-dependent covalent interactions between h+ and surface O atoms promote the structural disintegration of montmorillonite. *Langmuir* 41, 12607-12618. <https://doi.org/10.1021/acs.langmuir.5c00671>
- Yin, S.X., Zhang, J., 2005. Impacts of karst paleo-sinkholes on mining and environment in northern China. *Environ Geol* 48, 1077-1083. <https://doi.org/10.1007/s00254-005-0046-7>
- Zhang, H., Zhong, Y., Zhang, J., Zhang, Y., Kuang, J., Yang, B., 2020. Experimental research on deterioration of mechanical properties of carbonate rocks under acidified conditions. *J Petroleum Sci Eng* 185, 106612. <https://doi.org/10.1016/j.petrol.2019.106612>
- Zhang, Q., Zhang, X.Y., 2021. Cutting performance of shearer drum under different working conditions. *Chin J Appl Mech* 38, 2360-2368. <https://doi.org/10.11776/cjam.38.06.B216>
- Zhang, Y., Hu, M., Xu, W., Wang, H., Fan, L., Wang, R., Yan, L., Huang, W., Zhang, T., 2024. Experimental and model investigation on hydro-mechanical behaviour of sandy mudstone. *Eur J Environ Civil Eng* 28, 3004-3021. <https://doi.org/10.1080/19648189.2024.2330661>
- Zuo, J., Hong, Z., Peng, S., Shi, Y., Song, H., Li, M., Zhang, Z., 2019. Investigation on failure behavior of collapse column in China's coal mine based on discontinuous deformation numerical method. *PLoS One* 14, e0219733. <https://doi.org/10.1371/journal.pone.0219733>